Capturing Spatially Varying Anisotropic Reflectance Parameters using Fourier Analysis

Alban Fichet, Imari Sato, Nicolas Holzschuch

▶ **To cite this version:**

Alban Fichet, Imari Sato, Nicolas Holzschuch. Capturing Spatially Varying Anisotropic Reflectance Parameters using Fourier Analysis. Graphics Interface Conference 2016, Jun 2016, Victoria, BC, Canada. pp.65-73, 10.20380/GI2016.09 . hal-01302120v2

HAL Id: hal-01302120

https://inria.hal.science/hal-01302120v2

Submitted on 10 Jun 2016

HAL is a multi-disciplinary open access archive for the deposit and dissemination of scientific research documents, whether they are published or not. The documents may come from teaching and research institutions in France or abroad, or from public or private research centers.

L'archive ouverte pluridisciplinaire **HAL**, est destinée au dépôt et à la diffusion de documents scientifiques de niveau recherche, publiés ou non, émanant des établissements d'enseignement et de recherche français ou étrangers, des laboratoires publics ou privés.

Capturing Spatially Varying Anisotropic Reflectance Parameters using Fourier Analysis

Alban Fichet*
Inria ; Université de Grenoble/LJK ; CNRS/LJK

Imari Sato †
National Institute of Informatics

Nicolas Holzschuch ‡
Inria ; Université de Grenoble/LJK ; CNRS/LJK

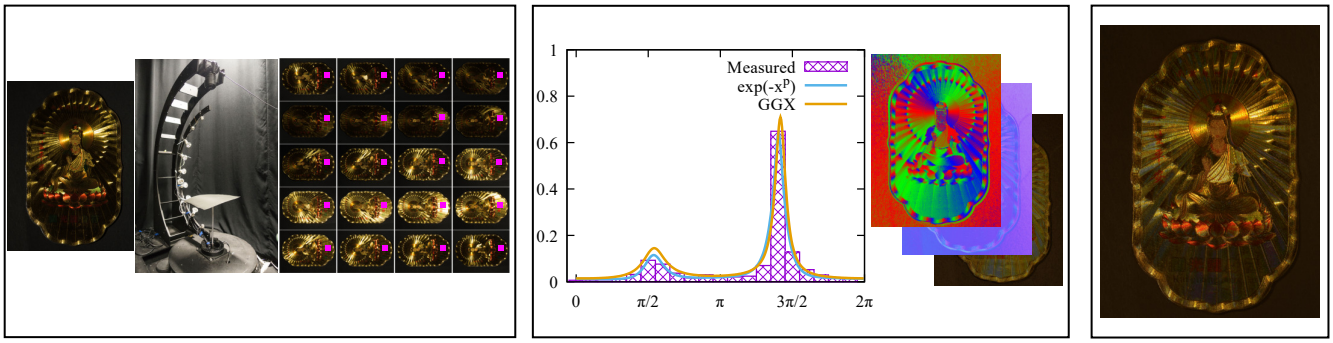

1. Capture 2. Analysis 3. Rendering

Figure 1: Our acquisition pipeline: first, we place a material sample on our acquisition platform, and acquire photographs with varying incoming light direction. In a second step, we extract anisotropic direction, shading normal, albedo and reflectance parameters from these photographs and store them in texture maps. We later use these texture maps to render new views of the material.

Abstract

Reflectance parameters condition the appearance of objects in photorealistic rendering. Practical acquisition of reflectance parameters is still a difficult problem. Even more so for spatially varying or anisotropic materials, which increase the number of samples required. In this paper, we present an algorithm for acquisition of spatially varying anisotropic materials, sampling only a small number of directions. Our algorithm uses Fourier analysis to extract the material parameters from a sub-sampled signal. We are able to extract diffuse and specular reflectance, direction of anisotropy, surface normal and reflectance parameters from as little as 20 sample directions. Our system makes no assumption about the stationarity or regularity of the materials, and can recover anisotropic effects at the pixel level.

Index Terms: I.3.7 [Computer Graphics]: Three-Dimensional Graphics and Realism—Color, shading, shadowing, and texture; I.4.1 [Image Processing and Computer Vision]: Digitization and Image Capture—Reflectance;

1 Introduction

Material reflectance properties encode how an object interact with incoming light; they are responsible for its aspect in virtual pictures. Having a good representation of an object material properties is essential for photorealistic rendering.

Acquiring material properties from real objects is one of the best way to ensure photorealism. It requires sampling and storing material reactions as a function of incoming light and viewing direction, a time-consuming process. Accurately sampling and storing a single material can take several hours with current acquisition devices.

Anisotropic materials show interesting reflection patterns, varying with the orientation of the material. Because the amount of light reflected depends on both the incoming light and observer orientation, the acquisition process is even more time-consuming for anisotropic materials. Similarly for spatially varying materials, where material properties change with the position on the object.

Measured materials require large memory storage, related to the number of sampled dimensions (up to 6 dimensions for spatially-varying anisotropic materials). For this reason, people often use analytic material models for rendering. Analytic BRDFs can also be authored and importance sampled more efficiently. Fitting parameters for these analytic materials to measured data is difficult; it is still an ongoing research project.

In this paper, we present a new method for acquisition of spatially varying anisotropic materials. We extract material parameters from a small set of pictures (about 20), with different lighting conditions but the same viewing condition. We use Fourier analysis to reconstruct material properties from the sub-sampled signal. We are able to extract diffuse and specular reflectance, direction of anisotropy, shading normal and reflectance parameters in a multi-step process. Our algorithm works with the anisotropic Cook-Torrance BRDF model, with several micro-facet distributions. The choice of the micro-facet distribution is left to the user, our algorithm automatically extracts the corresponding parameters. We make no assumptions about stationarity or regularity of the material, and recover parameters for each pixel independently. The spatial resolution of our algorithm is equal to the spatial resolution of the input pictures.

Our algorithm is described in Figure 1: we place a material sample on a rotating gantry, acquire a set of photographs for varying incoming light directions. From these photographs, we extract a set

*e-mail: Alban.Fichet@inria.fr
†e-mail: imarik@nii.ac.jp
‡e-mail: Nicolas.Holzschuch@inria.fr

of maps depicting reflectance parameters such as albedo, shading normal or anisotropic direction. These parameters are then used to generate new pictures of the material.

The remainder of this paper is organized as follows: in the next section, we briefly review previous work on material acquisition, focusing on acquisition of spatially varying or anisotropic materials. In section 3, we present our acquisition apparatus. In section 4, we describe our method for extracting reflectance parameters from the acquisition data. In section 5 we present acquisition results and evaluate the accuracy of our method. We discuss the limitations of our algorithm in section 6 and conclude in section 7.

2 Related Work

Acquiring material properties is time consuming, as it requires sampling over all incoming and outgoing directions. For spatially uniform materials, researchers speed up the acquisition process by exploiting this uniformity: a single photograph samples several directions, assuming the underlying geometry is known. Matusik *et al.* [16] used a sphere for isotropic materials. Ngan *et al.* [17] extended this approach to anisotropic materials using strips of materials on a cylinder. In these two approaches, the camera is placed far from the material samples so we can neglect parallax effects. Filip *et al.* [9] reverted the approach for anisotropic materials: they used a flat material sample, placed the camera close and exploited parallax effects for dense direction sampling.

These approaches do not work for spatially varying materials. A common technique is to precompute material response to illumination, then identify materials on their response to varying incoming light. Gardner *et al.* [10] a moving linear light source, combined with precomputed material response to identify spatially varying materials and normal maps. Wang *et al.* [23] identifies similar materials in the different pictures acquired and combines their information for a full BRDF measure. Dong *et al.* [6] extend the approach in a two-pass method: they first acquire the full BRDF data at few sample points, then use this data to evaluate the BRDF over the entire material using high-resolution spatial pictures. Compared to these methods, we do not make any assumptions about the homogeneity of the material, and recover material response independently at each pixel. Thus, we can acquire reflectance properties even for materials with high-frequency spatial variations (see Figure 1).

Ren *et al.* [18] begin by acquiring full BRDF information for some base materials. Samples of these materials are placed next to the material to measure, and captured together. By comparing the appearance of the known and unknown materials, they get a fast approximation of spatially varying reflectance. Their method is limited to isotropic reflectance.

Another promising area of research is to record material response to varying incoming light. Holroyd *et al.* [11] used spatially modulated sinusoidal light sources for simultaneous acquisition of the object geometry and isotropic material. Tunwattanapong *et al.* [21] used a rotating arm with LEDs to illuminate the object with spherical harmonics basis functions, allowing simultaneous recovery of geometry and reflectance properties. Aittala *et al.* [1] combined two different pictures of the same material (one with flash, the other without), then exploited the material local similarity to recover the full BRDF and normal map at each pixel. Their algorithm is limited to isotropic materials.

Empirical reflectance models represent the response by a material in a compact way. The most common models for anisotropic materials are anisotropic Ward BRDF [24] and the anisotropic Cook-Torrance BRDF [4]. The latter has a functional parameter, the distribution of normal micro-facets. Early implementations used a Gaussian distribution; in that case the Ward and Cook-Torrance models are very close. Recent implementations use different probability distributions. Brady *et al.* [3] used genetic programming to identify the best micro-facet distribution; they found that many measured materials are better approximated with a distribution in e^{-x^p} instead of a Gaussian.

Figure 2: Our acquisition platform: the sample and camera are static and aligned with each other, the light arm rotates around them. Arm position and picture acquisition are controlled by a computer.

3 Acquisition Apparatus

We have set up our own acquisition apparatus (see Figure 2): a flat material sample is placed on a console. The camera is vertically aligned with the sample normal, at a large distance. A rotating arm carrying lights provides varying lighting conditions.

The axis of rotation for the arm is equal to the view axis for the camera. A computer controls the arm position, which light sources are lit and the camera shooting, so the acquisition process is done automatically and can be conducted by a novice user.

For each acquisition we sample the incoming light direction regularly, with N samples, separated by $2\pi/N$.

We used a Nikon D7100 camera with a AF-S Nikkor 18-105 mm 1:3.5-5.6G ED lens. Shots were done in NEF format at 14 bits in no compression mode. We took 20 pictures for each material, corresponding to 20 samples in the incoming light direction.

Even though the camera and sample are fixed with respect to each other, the rotating arm movements induce small displacements in the pictures, of a few pixels between each frame. We align all the pictures before processing, using Enhanced Correlation Coefficient Maximization [7, 8], as implemented in OpenCV [2].

After this image registration and alignment, a given pixel in all the pictures corresponds to the same point on the material. We have for each pixel 20 samples corresponding to regularly sampled incoming light directions. We then extract material parameters at each pixel independently, using these samples.

4 Parameter Extraction

4.1 Reflectance Model

We make the hypothesis that the object surface is flat at the macroscopic level, but with small variations that can be encoded using a shading normal $\boldsymbol{n}_s = (\theta_n, \varphi_n)$. At every point on the surface, we define the main anisotropic direction. Angles in the tangent plane, such as φ_n, are measured with respect to this direction.

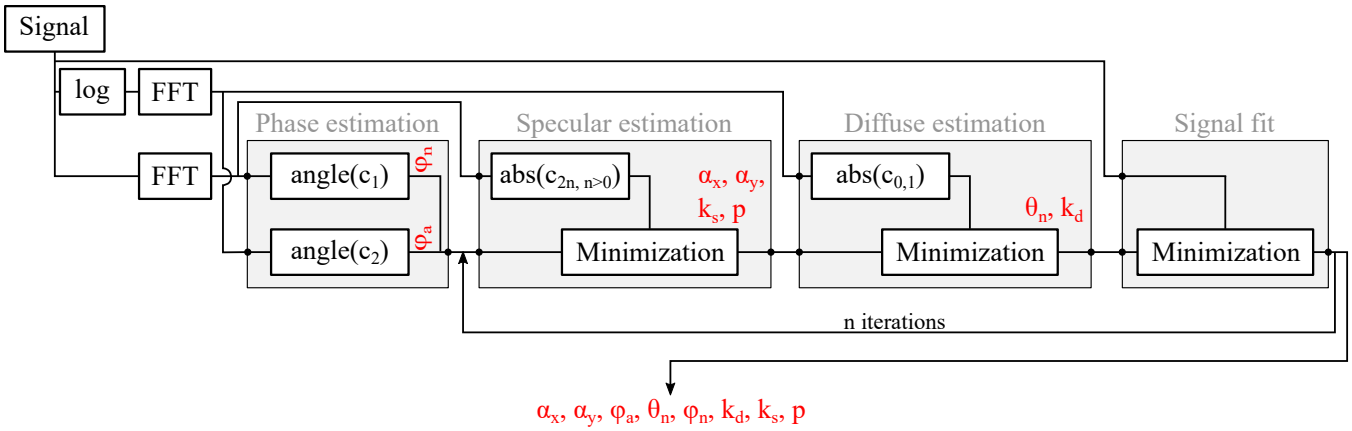

Figure 3: Our algorithm: first, we estimate the azimutal angle φ_n of the shading normal and the anisotropy direction φ_a using the phase shifts of the first and second harmonics. Then we estimate BRDF parameters by minimization: specular reflectance with even harmonics, diffuse reflectance and normal elevation with c_0 and c_1. In a final step, we perform minimization on the measured signal for minor adjustments on the parameters. For added accuracy, we can loop over the minimization process using computed parameters as input values.

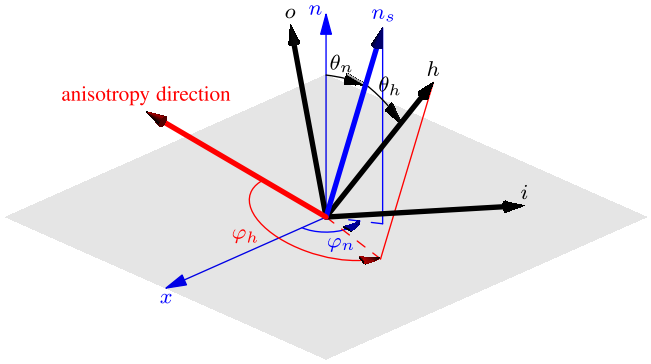

Figure 4: Notations for BRDFs: $\boldsymbol{i}$ is the incoming direction, $\boldsymbol{o}$ is the outgoing direction, $\boldsymbol{h}$ is the half-vector. θ_h is the angle between $\boldsymbol{h}$ and the shading normal, $\boldsymbol{n}_s$. φ_h is the angle between the half-vector and the main anisotropic direction on the tangent plane.

We assume that our material can be modelled using the anisotropic Cook-Torrance model [4], with a diffuse component:

$$\rho(\boldsymbol{i},\boldsymbol{o}) = \frac{k_d}{\pi} + \frac{k_s}{\alpha_x \alpha_y} \frac{F(\cos\theta_d) G(\boldsymbol{i},\boldsymbol{o})}{4\cos\theta_i \cos\theta_o} D\left(\tan^2\theta_h \left(\frac{\cos^2\varphi_h}{\alpha_x^2} + \frac{\sin^2\varphi_h}{\alpha_y^2}\right)\right) \tag{1}$$

Where:

- D is the micro-facet normal probability distribution. It is an open parameter. The original paper used a Gaussian: $D(x) = e^{-x}$. In this paper, we use two different distributions: GGX, introduced by Walter *et al.* [22] and $D(x) = e^{-x^p}$, introduced by Brady *et al.* [3].
- θ_h is the angle between the shading normal $\boldsymbol{n}_s$ and the half-vector $\boldsymbol{h} = (\boldsymbol{i}+\boldsymbol{o})/||\boldsymbol{i}+\boldsymbol{o}||$. θ_d is the angle between $\boldsymbol{h}$ and $\boldsymbol{i}$ (see Figure 4). φ_h is measured with respect to the main anisotropic direction.
- F is the Fresnel term, G is the shadowing and masking term,
- k_d and k_s are the diffuse and specular response, respectively.
- α_x and α_y are the main BRDF parameters and control the shape of the specular lobe. Isotropic BRDF correspond to $\alpha_x = \alpha_y$.

4.2 Main idea

We use a Fourier analysis of the signal for each pixel to extract the reflectance parameters: the *phase* of the Fourier coefficients gives us the direction of anisotropy, while their *amplitude* gives us the reflectance parameters. The Fourier analysis provides noise reduction to the signal; it is very efficient at identifying the direction of anisotropy.

More precisely, the phase of the second harmonics gives us the direction of anisotropy for the specular lobe, while the phase of the first harmonic gives the direction of anisotropy for the diffuse lobe, and thus for the normal.

We conduct the analysis independently for each pixel of the images, resulting in spatially varying information.

4.3 Fourier analysis for each pixel

For each pixel in the pictures from the acquisition setup, the contributions for all directions define a periodic signal of φ_h, $s(\varphi_h)$, which has been sampled N times. We use the Fourier transform of this signal, defined as the set of complex numbers c_n:

$$c_n = \int_0^{2\pi} s(\varphi_h) e^{ni\varphi_h} \, d\varphi_h \tag{2}$$

We compute the (c_n) using Fast Fourier Transform (FFT) [5].

If the shading normal is equal to the geometric normal, with our acquisition setting θ_h is a constant. Luminance information for a single pixel is only a function of φ_h, and more precisely a function of $\cos 2\varphi_h$. In that case, coefficients c_n for odd n are null. When the shading normal is different from the geometric normal, this assumption does not hold. We use this observation to separate the effects of the anisotropic BRDF and those of the shading normal: we fit the specular BRDF parameters using Fourier coefficients with even rank c_{2k}, and separately estimate the shading normal angle and diffuse BRDF parameters using the first two Fourier coefficients, (c_0, c_1).

In a final step, we fit all BRDF parameters together, using the entire model, and with the values computed using Fourier coefficients as starting points for parameters.

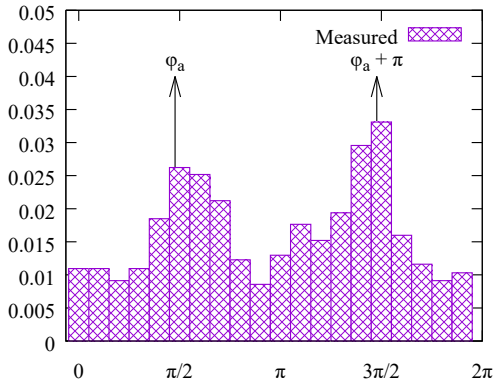

Figure 5: Extracting the anisotropic direction from the sampled signal, example for one pixel. Fourier analysis provides a robust answer even with a small number of samples and measurement noise.

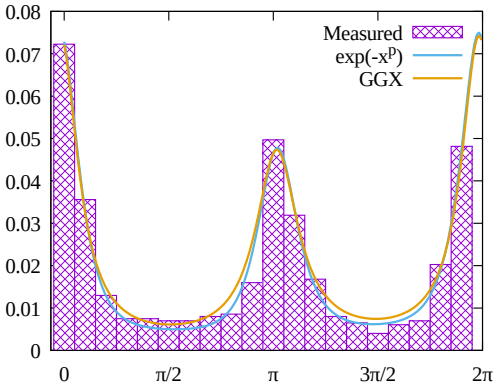

Figure 6: Extracting BRDF parameters from the sampled signal: we minimize the distance in Fourier space between the measured signal and the signal predicted by the BRDF models.

4.4 BRDF Anisotropic Direction

To estimate the anisotropic direction for the BRDF, we only consider the c_n for even numbers n, expressed as c_{2k}. All these Fourier coefficients are complex numbers, having a modulus d_{2k} and a phase β_{2k}:

$$c_{2k} = d_{2k} e^{i\beta_{2k}} \tag{3}$$

The angle φ_h in Equation 2 is expressed with respect to this local anisotropic direction. In the local frame, the anisotropic direction is expressed as an angle, φ_a. We compute the angle directly from the phase of the c_{2k} coefficients:

$$\varphi_a \equiv \frac{\beta_{2k}}{2k} \mod \pi/k \tag{4}$$

For example, with $k = 1$:

$$\varphi_a \equiv \beta_2 \mod \pi \tag{5}$$

Since φ_a is defined modulo π, Equation 5 defines it uniquely.

This extraction proves to be extremely robust, even with a small number of sampled directions (see Figure 5 and Figure 10).

4.5 Shading normal azimuthal direction

We use the c_1 Fourier coefficient to estimate the shading normal azimuthal direction: the reflected intensity is maximum when the incoming light is aligned with the shading normal. This has a 2π period; the phase of c_1 gives us the direction of this maximum.

4.6 Specular reflectance parameters

Once we have the anisotropic direction, we extract the remainder of the specular reflectance parameters from the even-numbered Fourier coefficients. In this step, we neglect the diffuse component.

We have one RGB color parameter k_s, two microfacet distribution parameters, α_x and α_y and potentially the exponent p if we use the $D(x) = e^{-x^p}$ distribution. We find the optimal set of parameters using a Levenberg-Marquadt optimisation on the Fourier spectrum [13, 15], as implemented by Lourakis [14].

For each set of parameter values $(k_s, \alpha_x, \alpha_y, (p))$, we compute the corresponding signal for all incoming light directions, then the Fast Fourier Transform of this signal, c'_n. On this estimated signal, all Fourier coefficients with odd rank are null by construction. We define the minimization error E in the optimisation process as the L_2 distance between the Fourier spectrum of the measured signal and the Fourier spectrum of the estimated signal over coefficients with even rank:

$$E = \sum_k |c_{2k} - c'_{2k}|^2 \tag{6}$$

For the fitting process, we observe that we have $\boldsymbol{n} = \boldsymbol{o}$, from our acquisition setup. Therefore $\cos\theta_o = 1$. $\cos\theta_i$ is also constant, and is known from the acquisition parameters. θ_h is also a constant, equal to $\theta_i/2$. This reduces the number of unknowns.

This optimisation converges quickly (less than 50 iterations for most of the pixels), and gives us the reflectance parameters for each pixel (see Figure 6).

For the Cook-Torrance BRDF model, the optimisation process gives us the value of the product $k_s F(\theta_d) G(\boldsymbol{i}, \boldsymbol{o})$. For our measuring angle, we can assume $G(\boldsymbol{i}, \boldsymbol{o}) \approx 1$. We will reconstruct the value of G at other angles from α_x and α_y using Smith's shadowing function [20]. With a single sample on θ_i, we do not have enough information to separate the Fresnel term from the specular reflectance and approximate it with a constant.

4.7 Diffuse component and shading normal

In a separate step, we fit the diffuse component of the BRDF k_d and shading normal angle θ_s using only the first two Fourier coefficients c_0 and c_1. As specular effects are functions of $\cos 2\varphi_h$, their influence on these Fourier coefficients is theoretically null, leaving only diffuse lighting. This step converges very quickly, because there is a small number of variables.

4.8 Control: fitting over the entire model and feedback loop

Our previous two fitting steps made several strong hypothesis, by separating shading normal and specular reflectance coefficients estimation. In practice, the shading normal and diffuse coefficients influence the specular BRDF coefficients. In a third step, we fit the entire BRDF model, with shading normal, diffuse and specular component with the full signal, using the values computed in the previous two steps as starting points.

Because the starting points are close to the actual position of the minimum, this step also converges quickly. At the end of this step, we have the full set of material parameters: BRDF values with diffuse component and shading normal.

For added accuracy, we loop over the whole fitting process, using the values we just computed: recompute parameters for the specular and diffuse part of the BRDF using the shading normal, fit the entire signal with the new specular and diffuse parameters. After two loops, our fitting process has converged to acceptable solutions.

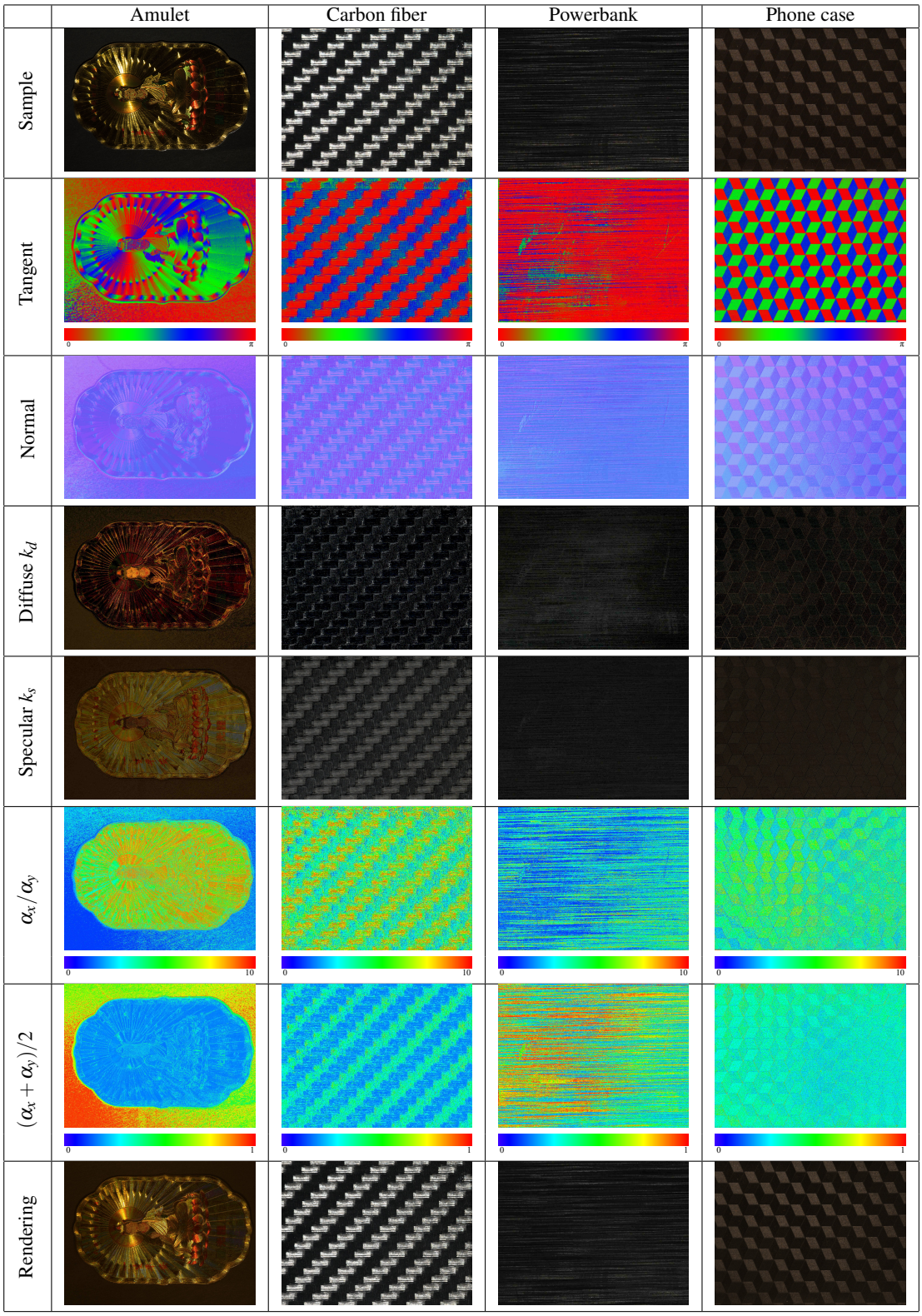

Figure 7: After extraction, we store BRDF parameters in textures: anisotropy direction (second row), shading normal (third row), diffuse and specular coefficients (k_d, k_s) and BRDF parameters (α_x, α_y, p). We visualise here the *anisotropy* of the material, α_x/α_y and its specularity, $(\alpha_x+\alpha_y)/2$. Our algorithm identifies the direction and amplitude of each material features. For a detailed view, see the zoomed-in insets in Figure 8.

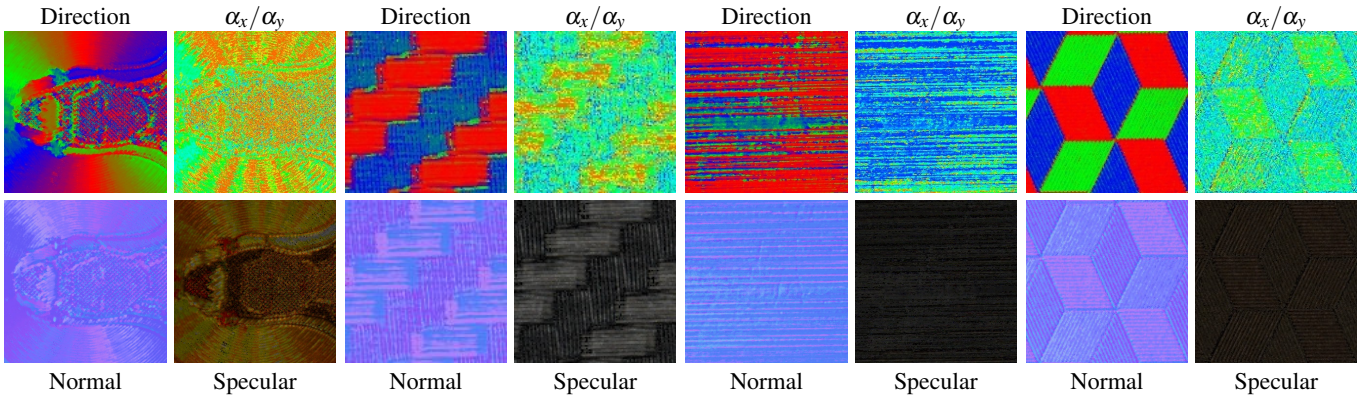

(a) Amulet (b) Carbon fiber (c) Powerbank (d) Phone case

Figure 8: Details of the extracted maps shown on Figure 7. For each sample, on the top left the anisotropic direction, on the top right, α_x/α_y, on the bottom left, the normal map and on the bottom right, the specular parameter k_s.

4.9 Storage and retrieval

After the full fitting process, we have for each pixel: the anisotropic direction, the shading normal and the BRDF parameters. We store these into several textures (see Figure 7 and 8), to be accessed at run time: anisotropic direction, shading normal, diffuse albedo, specular reflectance color and specular reflectance parameters (α_x, α_y, (p)). At run time, we retrieve these parameters and compute the reflectance value.

5 Results and Comparison

We have tested our extraction algorithm with different material samples and BRDF models. We captured reflectance data on four different materials:

- The *amulet* shows sharp variations in anisotropic directions, combined with smooth variations in diffuse reflectance, and is a difficult case for material acquisition.
- The *Carbon fiber* combines high frequency and low frequency material variations. It is an example of a woven material, with two principal anisotropic directions.
- The *Powerbank* is made of brushed aluminium, and exhibits strong anisotropy in a single direction.
- The *Phone case* has a repetitive pattern with three different anisotropic directions.

Our experiments show that the algorithm is extremely robust for parameter extraction, and works with a small amount of input photographs. Figure 7 shows the extracted parameters for our test materials; high-resolution pictures of the phone case material are available in the supplemental.

5.1 Numerical validation: anisotropic direction

Figure 5 shows the angular shift along with reflectance values for a single pixel of measured data. A strong advantage of Fourier analysis is its ability to identify the correct angular shift, even though it does not correspond to one of the sampled directions.

We also conducted tests on synthetic data: we generated data sets with known angular shift, sampled with 5 to 20 samples, and extracted the shift from the Fourier coefficients. Figure 10 shows the average difference between the actual shift and the retrieved value, as a function of the number of samples. The error falls below 1 degree for as little as 10 samples.

5.2 Numerical validation: analytic BRDFs

We tested our algorithm on analytic BRDFs, where the parameter values are known. Figure 11 shows an example. As you can see, the reconstructed signal provides a very good fit with the sample points.

5.3 BRDF parameters

Our algorithm also identifies BRDF parameters in a robust manner. Figure 7 shows the parameters retrieved from all our data sets: the shading normal, diffuse and specular coefficients, anisotropy direction and BRDF parameters. Instead of displaying directly the BRDF parameters α_x and α_y, we display the *anisotropy* and *specularity* of the BRDF. The former corresponds to the ratio α_x/α_y. It is equal to 1 for isotropic materials; the larger it is, the more prononced the anisotropy of the material. The latter corresponds to the average $(\alpha_x+\alpha_y)/2$. The smaller it is, the more specular the material.

Looking at the values for a single pixel (Figure 6), we see that the Fourier transform has filtered measure noise. The reconstructed reflectance values are not equal to the measured values, while keeping the main features of the signal.

We have tried our algorithm with two different micro-facet distributions: the GGX distribution [22] and the e^{-x^p} distribution [3]. Figure 6 shows a comparison between the BRDF values with these two distributions and the measured signal for a given pixel. Both are providing a good fit.

5.4 Computation time

Table 1 shows the overall computation time for each step in the algorithm, along with the average computation time per pixel. Although the average time per pixel is relatively low (6 ms to 9 ms, depending on the material), the high resolution of the pictures make the computation time several hours per material sample. Almost all this computation time is due to the parameter extraction using Levenberg-Marquadt. This fitting step is required, due to the non-linear nature of the BRDF and the small number of samples per pixel.

To reduce the computation time, we cropped the pictures to focus on the sampled material, removing as much as possible of the background material.

All these timings were recorded on a 2 processors 8-core Intel Xeon E5-2630 v3 at 2.40GHz, with 32Gb of RAM running Ubuntu 14.04 64bit with the kernel 3.19.0-25-generic. The Levenberg-Marquadt fitting library runs on 32 threads.

Table 1: Computation time for the different steps of our algorithm

Material	Alignment	Parameter Extraction	Resolution	Average per pixel
Amulet	12.8 s	36599 s	2299×1724 px	9.2 ms
Carbon fiber	3 s	2137 s	561×421 px	9.0 ms
Power bank	13 s	6177 s	1249×937 px	5.3 ms
Phone case	6 s	3870 s	949×712 px	5.7 ms

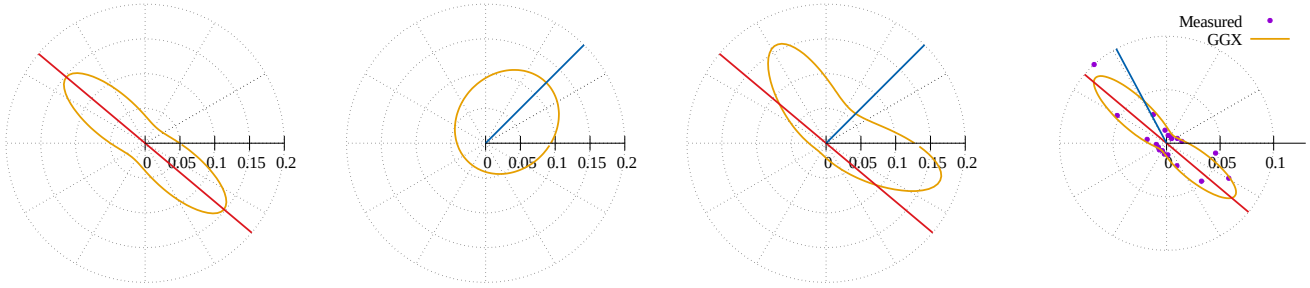

(a) Anisotropic BRDF with aligned normal (b) Isotropic BRDF with tilted normal (c) Anisotropic BRDF with tilted normal (d) Real data with fitting

Figure 9: Influence of the shading normal and the anisotropy on a theoretical signal. Red axis shows the anisotropic direction, blue line, the φ_n angle. The parametrization is reflectance on the radius as a function of φ_i. (a) theoretical anisotropic BRDF with the shading normal aligned with view and normal. (b) theoretical isotropic BRDF with a tilted shading normal. (c) combination of the tilted normal and the theoretical anisotropic BRDF. (d) signal extracted from a pixel on the phone case sample.

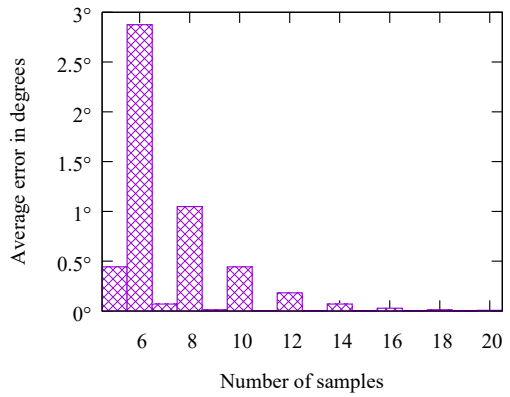

Figure 10: Difference between anisotropy direction and the value retrieved using the phase shift of c_2, as a function of the number of samples. Our algorithm retrieves an accurate value for the anisotropy direction even for small number of samples.

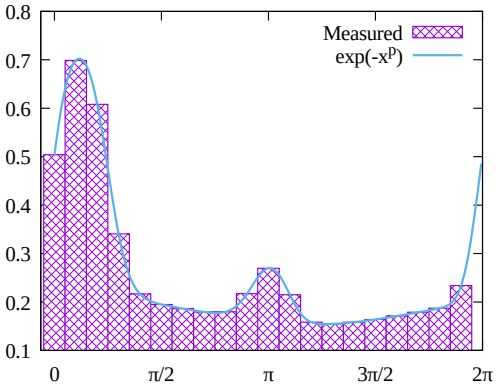

Figure 11: An example of fitted parameters using our algorithm on analytic BRDFs, with known parameters. The reconstructed version (blue curve) fits with the sampled data (bars).

5.5 Rendering

Figure 14 shows a side-by-side comparison between one of the pictures from the original dataset and a picture generated using the retrieved BRDF parameters. Of course, we can also generate pictures with different viewing directions and lighting conditions (see Figure 12 and the accompanying video). All these pictures show only local illumination and are rendered in real-time.

Once we have extracted BRDF parameters, we can also transfer the material to other objects and use them in global illumination settings. Figure 13 shows a virtual scene with materials extracted from the powerbank and phone case datasets, rendered using the Mitsuba renderer [12].

6 Discussion and Limitations

6.1 Shading normal

Our acquisition process is currently limited to planar objects. Identifying the shading normal enables use to acquire small variations in the local planarity of the object.

If the object is perfectly flat, with its normal aligned with the point of view ($\boldsymbol{o} = \boldsymbol{n}$), then the reflectance should be symmetric along the direction of anisotropy (see Equation 2 and Figure 9a). In practice, most of our measurements show a variation of amplitude between the two peaks of the signal (see Figures 1.2 and 6). Variations of the shading normal explain this difference of amplitude, but introduce a bias in our retrieval of the direction of anisotropy from the phase shift of the second harmonics, hence the need to conduct

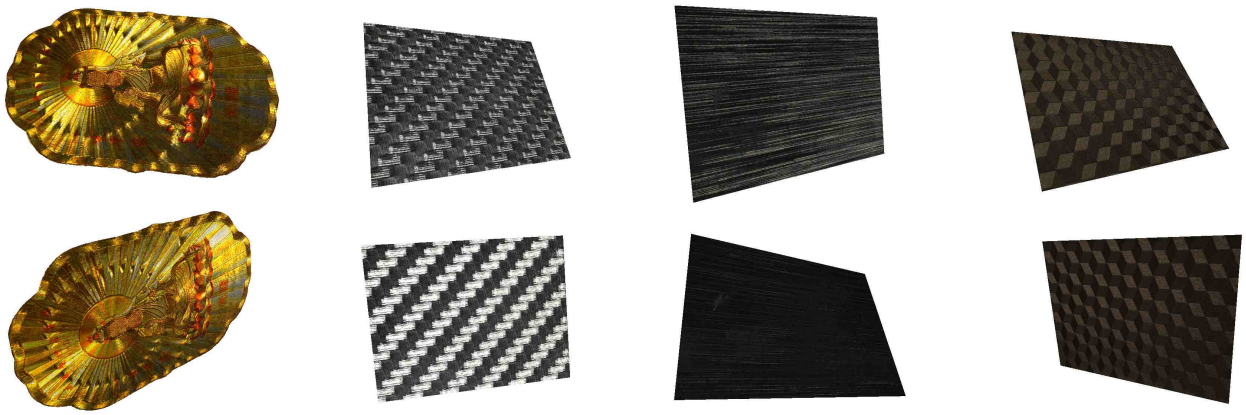

Figure 12: Picture of our four datasets under different viewing conditions, rendered in real-time.

Figure 13: We can transfer extracted material parameters to other objects and use them with global illumination. Left teapot with the carbon material, center one with the powerbank material and left one with the phone material.

(a) Original picture

(b) Reconstructed picture with identical viewing and lighting direction

Figure 14: Comparison between original picture and picture reconstructed from the extracted BRDF. See also Figure 7.

a final fitting step on the entire signal.

Figure 9 illustrates the influence of the different sources of anisotropy. We represent the BRDF intensity in polar coordinates, as a function of φ_h, with $\boldsymbol{o} = \boldsymbol{n}$. With a flat surface and anisotropic BRDF, the signal is symmetric along both the direction of anisotropy and the orthogonal direction (Figure 9a). With a shading normal and isotropic BRDF, the signal is symmetric along the shading normal (Figure 9b). With a combination of shading normal and anisotropic BRDF, there is no symmetry (Figure 9c). Signal measured on our test scenes exhibit the same behaviour (Figure 9d).

In our analysis, we constrained the angle between shading normal and geometric normal θ_n to remain below a certain threshold (20°). As θ_n increases, it becomes harder for our method to retrieve anisotropy. An extension to curved objects would require a different method to identify the direction of the normal, and more samples over the incoming light elevation.

6.2 Limitations

The main advantage of our acquisition process is the robustness and spatial accuracy. We treat each pixel independently, with only a small number of sampled pictures, and still retrieve enough information to reproduce the aspect of the material. We can handle pixel-size features in the measured data: the spatial resolution of the output is equal to the spatial resolution of the input photographs.

The drawbacks are related to the limited amount of information: we cannot retrieve the Fresnel term with only one set of measurements, with constant angle for incoming light. This reduces the accuracy of our reflectance model near grazing angles. This limited amount of samples also limits the ability to deal with highly specular materials. As matter of fact, due to Nyquist-Shannon sampling theorem, highly specular material will have higher frequencies in the Fourier domain which are going to be represented as lower frequency contributions with a limited amount of samples. This explains the error observed in the amulet sample. Although we have limited our capture with twenty samples in this paper, our algorithm can work with higher number of samples.

Finally, our entire acquisition process assumes anisotropic reflectance with a single anisotropic lobe. Reflectance with two anisotropic lobes, as exhibited by Filip *et al.* [9] would require a

different approach.

7 Conclusion and Future Work

We have presented a complete system for rapid acquisition of spatially varying anisotropic materials. Our system works by taking several pictures of the material sample, then extracting anisotropic direction and material properties at each pixel using Fourier analysis.

Our system is stable and robust, and produces noise-free parameter maps, even with a small number of sampled directions. We extract material properties at a high resolution, at the pixel level. Our system lets designers reuse the sampled material on virtual objects.

In future work, we would like to improve the accuracy of our system by merging together data sampled from neighbouring points with similar material, after shifting it in the angular direction to take into account their anisotropy. We also plan to extend the approach to non-planar material samples, retrieving simultaneously normal directions and reflectance parameters.

Acknowledgements

This work was funded in part by an ANR grant ANR-15-CE38-0005 "Materials" and by a Grant-in-Aid for Scientific Research on Innovative Areas (No.15H05918) from MEXT, Japan.

References

[1] M. Aittala, T. Weyrich, and J. Lehtinen. Two-shot SVBRDF capture for stationary materials. *ACM Trans. Graph.*, 34(4):110:1–110:13, July 2015.

[2] G. Bradski. The OpenCV library. *Dr. Dobb's Journal of Software Tools*, 25(11):120–126, Nov. 2000.

[3] A. Brady, J. Lawrence, P. Peers, and W. Weimer. genBRDF: Discovering new analytic BRDFs with genetic programming. *ACM Trans. Graph.*, 33(4):114:1–114:11, July 2014.

[4] R. L. Cook and K. E. Torrance. A reflectance model for computer graphics. *ACM Trans. Graph.*, 1(1):7–24, 1982.

[5] J. W. Cooley and J. W. Tukey. An algorithm for the machine calculation of complex Fourier series. *Math. Comp.*, 19:297–301, 1965.

[6] Y. Dong, J. Wang, X. Tong, J. Snyder, Y. Lan, M. Ben-Ezra, and B. Guo. Manifold bootstrapping for SVBRDF capture. *ACM Trans. Graph.*, 29(4):98:1–98:10, July 2010.

[7] G. Evangelidis and E. Psarakis. Parametric Image Alignment Using Enhanced Correlation Coefficient Maximization. *IEEE Transactions on Pattern Analysis and Machine Intelligence*, 30(10):1858–1865, Oct. 2008.

[8] G. Evangelidis and E. Psarakis. Projective Image Alignment by using ECC Maximization. In *Int. Conf. on Computer Vision Theory and Applications (VISSAP)*, Jan. 2008.

[9] J. Filip, R. Vavra, and M. Havlicek. Effective acquisition of dense anisotropic BRDF. In *International Conference on Pattern Recognition (ICPR)*, pages 2047–2052, Aug. 2014.

[10] A. Gardner, C. Tchou, T. Hawkins, and P. Debevec. Linear light source reflectometry. *ACM Trans. Graph.*, 22(3):749–758, July 2003.

[11] M. Holroyd, J. Lawrence, and T. Zickler. A coaxial optical scanner for synchronous acquisition of 3D geometry and surface reflectance. *ACM Trans. Graph.*, 29(4):99:1–99:12, July 2010.

[12] W. Jakob. Mitsuba renderer, 2010. http://www.mitsuba-renderer.org.

[13] K. Levenberg. A method for the solution of certain problems in least squares. *Quart. Appl. Math.*, 2:164168, 1944.

[14] M. Lourakis. levmar: Levenberg-marquardt nonlinear least squares algorithms in C/C++. `http://www.ics.forth.gr/~lourakis/levmar/`, July 2004.

[15] D. Marquadt. An algorithm for least squares estimation on nonlinear parameters. *SIAM J. Appl. Math.*, 11:431–441, 1963.

[16] W. Matusik, H. Pfister, M. Brand, and L. McMillan. A data-driven reflectance model. *ACM Transactions on Graphics*, 22(3):759–769, July 2003.

[17] A. Ngan, F. Durand, and W. Matusik. Experimental analysis of BRDF models. In *Eurographics Symposium on Rendering*, pages 117–226, 2005.

[18] P. Ren, J. Wang, J. Snyder, X. Tong, and B. Guo. Pocket reflectometry. *ACM Trans. Graph.*, 30(4):45:1–45:10, July 2011.

[19] S. Rusinkiewicz. A new change of variables for efficient BRDF representation. In G. Drettakis and N. Max, editors, *Rendering Techniques '98 (Eurographics Rendering Workshop)*, pages 11–22, 1998.

[20] B. Smith. Geometrical shadowing of a random rough surface. *IEEE Transactions on Antennas and Propagation*, 15(5):668–671, Sept. 1967.

[21] B. Tunwattanapong, G. Fyffe, P. Graham, J. Busch, X. Yu, A. Ghosh, and P. Debevec. Acquiring reflectance and shape from continuous spherical harmonic illumination. *ACM Trans. Graph.*, 32(4):109:1–109:12, July 2013.

[22] B. Walter, S. Marschner, H. Li, and K. E. Torrance. Microfacet models for refraction through rough surfaces. In *Eurographics Symposium on Rendering*, 2007.

[23] J. Wang, S. Zhao, X. Tong, J. Snyder, and B. Guo. Modeling anisotropic surface reflectance with example-based microfacet synthesis. *ACM Trans. Graph.*, 27(3):41:1–41:9, Aug. 2008.

[24] G. J. Ward. Measuring and modeling anisotropic reflection. *SIGGRAPH Comput. Graph.*, 26(2):265–272, July 1992.